Published in final edited form as:
Biochemistry. 2012 January 31; 51(4): 917–925. doi:10.1021/bi201662k.

The *Streptomyces*-produced antibiotic fosfomycin is a promiscuous substrate for Archaeal isopentenyl phosphate kinase

Mark F. Mabanglo[1], **Adrian W. R. Serohijos**[2], and **C. Dale Poulter**[1]

[1]Department of Chemistry, University of Utah, 315 South 1400 East Salt Lake City, Utah 84112 USA

[2]Department of Chemistry and Chemical Biology, Harvard University, 12 Oxford Street, Cambridge, Massachusetts 02138 USA

Abstract

Isopentenyl phosphate kinase (IPK) catalyzes the phosphorylation of isopentenyl phosphate to form the isoprenoid precursor isopentenyl diphosphate (IPP) in the archaeal mevalonate pathway. This enzyme is highly homologous to fosfomycin kinase (FomA), an antibiotic resistance enzyme found in a few strains of *Streptomyces* and *Pseudomonas* whose mode of action is inactivation by phosphorylation. Superposition of *Thermoplasma acidophilum* (THA) IPK and FomA structures aligns their respective substrates and catalytic residues, including H50 and K14 in THA IPK, and H58 and K18 in *S. wedmorensis* FomA. These residues are conserved only in the IPK and FomA members of the phosphate subdivision of the amino acid kinase superfamily. We measured the fosfomycin kinase activity of THA IPK, K_m = 15.1 ± 1.0 mM and k_{cat} = (4.0 ± 0.1) × 10^{-2} s^{-1}, resulting in a catalytic efficiency, k_{cat}/K_m = 2.6 $M^{-1}s^{-1}$, that is five orders of magnitude less than the native reaction. Fosfomycin is a competitive inhibitor of IPK, K_i = 3.6 ± 0.2 mM. Molecular dynamics simulation of the IPK•fosfomycin•MgATP complex identified two binding poses for fosfomycin in the IP binding site, one of which results in a complex analogous to the native IPK•IP•ATP complex that it engages H50 and the lysine triangle formed by K5, K14, and K205. The other binding pose leads to a dead-end complex that engages K204 near the IP binding site to bind fosfomycin. Our findings suggest a mechanism for acquisition of FomA-based antibiotic resistance in fosfomycin producing organisms.

Modern enzymes are commonly understood to be highly specific towards the substrates and chemical transformations that they catalyze. This selectivity underlies catalysis in biology. Enzyme selectivity prevents the conversion of unintended substrates that wastes cellular energy or has other deleterious effects on the organism in a cell where the chemical structures of metabolites are similar and where cross wiring of metabolic pathways exists (1). In contrast, primordial enzymes likely possessed a substantial degree of ambiguity with respect to binding and catalysis to generate a variety of products (2). These features are conducive for evolution new enzymes by gene duplication and optimization (2–4). In an organism under environmental stress, which potentially requires new reactions to survive, enhanced specificity can be selected by evolution. Low levels of promiscuous activities, *i.e.* those different than the main function, may persist in a specialized enzyme if they are not

Corresponding Author: poulter@chem.utah.edu. Telephone: (801) 581-6685.

ASSOCIATED CONTENT. Supporting Information. Detailed experimental procedures for competitive inhibition experiments and site-directed mutagenesis of THA IPK, Michaelis-Menten curves and Lineweaver-Burk graphs, sequence and structural alignments, and complete list of authors for reference 21 are supplied. This material is available free of charge via the Internet at http://pubs.acs.org.

detrimental to the organism, and there is no selective pressure for their elimination (5). In some cases promiscuous activity can complement gene deletions in metabolic pathways, for example in *E. coli phn* operon knockouts by recruitment of the phosphite-dependent hydrogenase activity of alkaline phosphatase (6), or *E. coli* auxotrophs that utilize promiscuous sugar kinases encoded by cryptic genes to rescue glucokinase deficient mutants (7). It has been suggested that promiscuity is an innate characteristic of all enzymes rather than an anomaly, and that there is a multitude of promiscuous activities extant in living cells available for exploitation by the host.

Recently, Mabanglo *et al.* reported the structures of isopentenyl phosphate kinase (IPK) in ternary complexes with its substrates and products (8). This enzyme is found only in *Archaea*, where it catalyzes the ATP-dependent phosphorylation of isopentenyl phosphate (IP) in the alternate mevalonate pathway (Scheme 1a). IPK is a member of the amino acid kinase (AAK) family of enzymes that phosphorylates small molecules with carboxylate, carbamate, phosphate and phosphonate moieties (8, 9). In this family, IPK and the bacterial resistance protein fosfomycin kinase (FomA) in *Streptomyces* have very high structural homology despite significant sequence divergence (22–25% identity) (Figure 1a) (10). The two enzymes possess a catalytic lysine triad, the lysine triangle, and an active site histidine residue that are not found in other members of the phosphate/phosphonate subdivision (Figure 1b) (8, 9). Thus, it was suggested that the *ipk* gene was the source of *fomA*, presumably acquired by fosfomycin producing strains of *Streptomyces* and *Pseudomonas* by horizontal gene transfer, and converted into a specialized fosfomycin kinase through mutation and selection (8, 11). This scenario is consistent with acquisition of resistance in bacteria constantly exposed to an antibiotic (12). In the case of *Streptomyces*, fosfomycin kinase activity was added to other resistance strategies in its arsenal (Scheme 1b), which includes fosfomycin inactivation by opening of the oxirane ring catalyzed by the metalloenzymes FosA, FosB and FosX (13–16).

We tested IPK from *Thermoplasma acidophilum* (THA IPK) for fosfomycin kinase activity and discovered that the antibiotic is an alternate substrate for the enzyme, albeit with poorer binding affinity and a reduced rate of turnover. Moreover, fosfomycin is a competitive inhibitor of isopentenyl phosphate kinase activity. Using molecular dynamics simulations, we discovered a binding mode for fosfomycin similar to that of IP that forms a stable complex with IPK, in addition to a separate binding mode that forms a dead-end complex.

EXPERIMENTAL PROCEDURES

Product turnover assay using γ-[^{32}P] ATP

The phosphorylation of fosfomycin by IPK was visualized by incubating the enzyme in assay buffer (100 mM HEPES pH 7.5 containing 10 mM $MgCl_2$, 10 mM β-mercaptoethanol, 1 mg/mL BSA, γ-[^{32}P] ATP and varying concentrations of fosfomycin at 37 °C for 10 min. Each reaction was quenched with 113 uL of methanol/750 mM EDTA (100:13 v/v). Samples (5 μL) were spotted on silica plates and developed with $CHCl_3$/pyridine/formic acid/H_2O (30:70:16:10 v/v/v/v). The TLC plate was imaged for 24 h using a storage phosphor autoradiography cassette and visualized using a Typhoon 8600 variable mode imager (GE Healthcare). The same procedure was used in the parallel comparison of the products formed by *S. wedmorensis* FomA and THA IPK, except that 10 mM fosfomycin and 10 μM of each enzyme was used in the incubations.

MS/MS fragmentation of fosfomycin phosphate product

The presence of fosfomycin phosphate was confirmed by performing MS/MS fragmentation on the ammonium form of fosfomycin phosphate (mass = 236) produced by THA IPK and

S. wedmorensis FomA. The products were obtained by incubating 20 μM of each enzyme in assay buffer (100 mM HEPES pH 7.5, 1 mg/mL BSA, 10 mM β-mercaptoethanol, 10 mM $MgCl_2$) containing 25 mM fosfomycin at 37 °C for 2 hr, in a total volume of 1 mL. The enzymes were removed by centrifugation using a 10, 000 MWCO Centricon, and the filtrate was flash frozen in liquid N_2 and lyophilized overnight in 1.5 mL microfuge tubes. The resulting slurry was dissolved in 100 μL of 25 mM NH_4HCO_3 pH 7.5 and submitted for MS/MS fragmentation.

Steady state kinetics of the IPK-fosfomycin reaction

The protocol for fluorescent assays was based on the procedure by Pilloff *et al.* with slight modifications (17). The activities of coupling enzymes were determined by measuring the change in absorbance of NADH at 339 nm. Different concentrations of lactate dehydrogenase (LDH) were mixed in the assay buffer (100 mM HEPES containing 10 mM $MgCl_2$, 10 mM β-mercaptoethanol, 1 mg/mL BSA, 120 μM pyruvate and 150 μM NADH) at 37 °C. For pyruvate kinase, different concentrations of the coupling enzyme were mixed in assay buffer (100 mM HEPES containing 10 mM $MgCl_2$, 10 mM β-mercaptoethanol, 1 mg/mL BSA, 1 mM PEP, 4 mM ADP, 150 μM NADH and LDH) at 37 °C. The enzymatic rates in AU/s where converted to specific activity units (U/mL) by using the NADH extinction coefficient $\varepsilon = 6.22\ mM^{-1}\ cm^{-1}$. To initiate the reaction, IPK was added to the assay buffer (100 mM HEPES pH 7.5 containing 10 mM $MgCl_2$, 10 mM β-mercaptoethanol and 1 mg/mL BSA) including appropriate amounts of coupling enzymes and fosfomycin (or the native substrate IP for positive control reactions) in a final volume of 200 μL. The reaction was monitored at 37 °C for 600 s by observing the change in fluorescence (λ_{ex} = 340 nm, λ_{em} = 460 nm) (FluoroMax, Jobin Yvon Horiba). Background rates were measured at different concentrations of fosfomycin in the absence of the enzyme and were averaged. The initial rates were measured from the linear portion of the curve (< 15 % consumption of the concentration-limiting substrate). The kinetic constants were determined by fitting the matrices of initial rates to equation 1 using Grafit 5 (Erithacus Software) (18):

$$v = V_{max}[A][B]/K_d^{A}K_m^{B} + K_m^{B}[A] + K_m^{A}[B] + [A][B] \quad (1)$$

where A and B are fosfomycin and ATP, V_{max} is the maximum rate, K_m is the Michaelis-Menten constant and K_d is the enzyme dissociation constant. The lag time τ of the coupled assay is given by the equation

$$\tau = K_m^{ADP}/V^{PK} + K_m^{Pyr}/V^{LDH} \quad (2)$$

where K_m^{ADP} = 0.3 mM according to Sigma and K_m^{Pyr} = 0.164 mM according to Zewe and Fromm (19) and V is the activity of the enzyme in U/mL. The lag time τ of the reaction was then chosen to be less than 10 s, which ensured that the system reached 99 % of the steady state rate of ADP production in 45 s according to the equation

$$dP/dt = v_0(1 - e^{-t/\tau}) \quad (3)$$

where v_0 is the steady state rate and t and τ are in min.

Molecular dynamics simulations of the IPK•fosfomycin•MgATP complex

We performed molecular dynamics simulations using GROMACS (20) with CHARMM27 (21) force field for proteins and small molecules (22) and TIP3P (23) for water. The initial structure of the kinase is derived from the crystal structure of IPK, while the specific binding

pose of ligands in the binding pocket of IPK• fosfomycin•MgATP was derived from the superposition of structures 3LKK (IPK) and 3D41(FomA) from the Protein Data Bank. The missing loop and αF helix of IPK (residues 189–201) were modeled based on sequence and structure alignment with NAGK (1GS5) (24) where the corresponding secondary structures in the latter most approximate the length of these missing regions (Figure S1, S2). The geometry of the modeled secondary structures was validated using Molprobity (25). After an initial rapid energy minimization, the system was equilibrated by performing a position-restrained NVT simulation for 100 ps followed by an NPT run for another 100 ps. We then performed an unconstrained production run for 30 ns to validate the initially hypothesized poses of fosfomycin and MgATP. Long-range electrostatics was treated with Particle Mesh Ewald (26) with grid spacing of 12 Å and a cutoff of 10 Å. We used the modified Berendsen (27) and Parrinello-Rahman (28) algorithms for temperature and pressure couplings, respectively. The same experiments were performed on the native IPK•IP•MgATP complex as a control.

RESULTS

Detection of fosfomycin kinase activity

Autoradiography studies using γ-[^{32}P] ATP showed that fosfomycin is an alternate substrate for IPK. The formation of the product was accompanied by a concomitant decrease in γ-[^{32}P] ATP when the concentration of fosfomycin was in the high μM to mM range (Figure 2a). In contrast, K_m^{IP} = 4.4 μM for THA IPK. The product of the promiscuous reaction, assigned as fosfomycin phosphate, is consistent with the intense spot with R_f = 0.14 relative to IPP, R_f = 0.37. This spot did not appear in control reactions containing only IP or γ-[^{32}P] ATP and IPK. In addition, parallel incubation of *S. wedmorensis* FomA and IPK showed product spots with the same R_f s as above (Figure 2b). These product spots were not found in incubations containing neither enzymes nor fosfomycin substrate. MS/MS fragmentation of the ammonium form of fosfomycin phosphate (mass = 236) from incubations with THA IPK (Figure 3a) and *S. wedmorensis* FomA (Figure 3b) resulted in identical fragmentation patterns. Positive ion species corresponding to $[C_3H_5O]^+$ (mass = 57), $[C_3H_6O_3P]^+$ (mass = 121), $[H_4O_4P]^+$ (mass = 99), and $[C_3H_8O_4P]^+$ (mass = 139) were found in the fragmentations of the products of both enzymes. The first two cations, $[C_3H_5O]^+$ and $[C_3H_6O_3P]^+$ were also observed in the fragmentation of a fosfomycin standard (Figure S3).

In ^{31}P NMR assays, resonances corresponding to a phosphonate-phosphate moiety were not detected owing to the slow reaction and an apparently unfavorable equilibrium between fosfomycin-ATP and fosfomycin phosphate-ADP. We initially attempted longer incubation times without success. The autoradiogram shows a byproduct of the kinase reaction whose R_f is similar to that of IPP (Figure 2a), which is more pronounced in the absence of fosfomycin (Figure 2b, lane 4). Chen and Poulter (10) had previously shown that this by-product is $^{32}P_i$, resulting from the combined effects of γ-[^{32}P] ATP degradation and the intrinsic ATPase activity of IPK. ATPase activity has been observed in many kinases and is commonly negligible compared to native kinase activities (28), although in some cases is sufficiently large to interfere with their precise measurements (29). The ATPase activity of THA IPK was found to be sufficiently small (~ 200 times slower) that it did not interfere with measurements of the promiscuous fosfomycin kinase activity.

Kinetic constants

Initially, a series of fosfomycin concentrations from 750 μM to 80 mM was used to measure the apparent kinetic constants of the reaction at a saturating 250 μM concentration of ATP (data not shown) in order to identify a suitable range of concentrations for kinetic measurements. Initial rates were fitted to the equation for bi-substrate reactions (Figure S4a)

and were transformed to a Lineweaver-Burk plot (Figure S4b). The fosfomycin kinase reaction proceeds by the same sequential mechanism seen for IP and ATP. The kinetic constants for phosphorylation of IP and fosfomycin are summarized in Table 1.

Fosfomycin is a competitive inhibitor of IPK

Superposition crystal structures of the THA IPK and FomA ternary complexes show a close alignment of their respective IP and fosfomycin substrates (Figure 1b) suggesting that fosfomycin will be a competitive inhibitor of the faster IP kinase reaction. The best fit of our kinetic data was obtained with the equation for competitive inhibition (Equation 1, Supporting Information). The Michaelis-Menten curves (Figure S5a) showed an apparent increase in K_m^{IP} with increasing inhibitor concentration, which was overcome at high concentrations of IP. The Lineweaver-Burk transformation of these curves showed showed typical competitive behavior (Figure S5b), with $k_{cat} = 7.5\ s^{-1}$ and $K_i = 3.6 \pm 0.20$ mM. Weak inhibition of THA IPK by fosfomycin is consistent with K_m for fosfomycin and is probably due to the incompatibility of its polar epoxide group with the hydrophobic pocket tailored for the isoprene unit in IP.

Binding poses for FomA in IPK

Similar structures for the ternary complexes of IPK and FomA suggest that the native substrate IP and the promiscuous substrate fosfomycin adopt similar binding poses in IPK. To examine this issue, we performed molecular dynamics simulations on the IPK•fosfomycin•MgATP and IPK•IP•MgATP ternary complexes. To fix the MgATP ligand in its binding site during simulation, an accurately modeled structure for the missing αF-αG loop and αF helix of IPK was supplied to the starting structure based on the aligned sequences of IPK from *T. acidophilum* and *M. thermautotrophicus* (8), *S. wedmorensis* FomA (10) and *E. coli* NAGK (24) (Figure S1 and S2). These alignments indicate that the secondary structure in NAGK, which only differs from the sequence in THA IPK by a single amino acid, can be used to model the missing loop and αF helix in IPK. The system is stable and has an average Cα RMSD of 1.5 Å with respect to the starting structure (Figure 4a, left and right panels). We computed the heavy atom RMSD of fosfomycin and ATP and found two stable conformers of fosfomycin in the binding pocket (Figure 4b, left panel). The normalized RMSD distributions support the observed two-state conformations (Figure 4b, right panel). Closer inspection of these two conformations shows that fosfomycin binds to the N-terminal lobe of THA IPK that contains the IP binding site (Figure 4c).

In both IPK•fosfomycin•MgATP structures, fosfomycin obstructs the IP binding site, as expected for a competitive inhibitor. Moreover, the MgATP conformation is essentially fixed while fosfomycin is translated by 3.9 Å in the first pose and 4.8 Å in the second relative to the position occupied by IP, presumably to reduce unfavorable interactions between the polar epoxide and the hydrophobic binding pocket. In the first binding pose (Figure 4d), the oxygen of the epoxide is oriented toward the solvent region, while the methyl group packs into the hydrophobic pocket. The catalytic residue H50 in the αB helix forms a hydrogen bond with the phosphonate group, analogous to its interaction with IP. This places a phosphonate oxygen in fosfomycin ~5.1 Å from the γ phosphorus in ATP. This is substantially longer than the 2.9 Å distance between a non-bridging oxygen in IP and the ATP γ phosphorus in the IPK ternary complex (3LKK) and likely contributes to the low rate of the promiscuous reaction. However, the distance between the phosphonate oxygen and the ATP γ phosphorus in the structure of the FomA•fosfomycin•MgATP complex, modeled from coordinates of the FomA•MgATP (3QUN) and the FomA•fosfomycin•ATP (3QUO) complexes, is 4.0 Å (Figure 1b) (31). Thus, it is likely that this distance is a good approximation of the real phosphonate-γ phosphate distance. Examination of this binding pose also indicates that the active site Mg^{2+} is located 3.7 Å from a phosphonate oxygen,

perhaps facilitating nucleophilic attack on ATP. This interaction as well as innate enzyme plasticity could help overcome longer distance between reactive phosphonate and phosphate centers in IPK•fosfomycin•MgATP. Interactions involving K5, K14, K205 and D144 observed in the IPK•IP•ATP crystal structure (8) and those of corresponding residues in FomA (31) are essentially conserved in this binding pose. Mutagenesis studies of these residues in FomA are consistent with their expected roles in binding and catalysis (31), suggesting that the first binding mode is a productive one.

In the second, less populated binding state, fosfomycin is removed even farther away from the IP location in the active site. The hydrogen bonding of the phosphonate moiety and H50 is absent. New hydrogen bonds are seen between the epoxide group and S142 and between a phosphonate oxygen and K204 in the αG helix. In THA IPK, S142 binds a phosphate oxygen in IP. This residue is conserved in FomA and orients the phosphonate moiety in fosfomycin for nucleophilic attack on ATP (31). In addition, the closest phosphonate oxygen is 6.3 Å away from the γ phosphorus in ATP and 4.1 Å from Mg^{2+} in this second pose (Figure 4e).

Molecular dynamics simulation of IPK•IP•MgATP showed that the complex is stable (Figure S6a) and revealed a single binding pose with IP and MgATP virtually unchanged from their respective poses in the crystal structure (Figure S6b). The latter result suggests that the crystal structure closely approximates the structure of the complex in solution and also lends credence to the two calculated binding poses of fosfomycin in the IPK active site.

The K204A mutant IPK has fosfomycin activity comparable to the wild type IPK

Structures from crystallography and dynamics calculations suggest that K204 does not play a major role in catalysis. Recruitment of K204 to form a hydrogen bond to an oxygen atom of the phosphonate moiety in the second fosfomycin pose appears to replace the hydrogen bond between H50 and a phosphonate oxygen, leading to a dead end complex. The His_6-tagged K204A mutant was prepared, purified, and assayed for fosfomycin kinase activity. The mutant phosphorylated fosfomycin, and the kinetic constants for the reaction were very similar to those for wild type IPK (Table 1, Figure S7a and Figure S7b). In addition, mutation did not significantly alter the kinetic constants for the native reaction (Table 1) (11).

DISCUSSION

Fosfomycin is a secondary metabolite produced in several species of *Streptomyces* (32) and *Pseudomonas* (33) that is used clinically to treat cystitis (34) as well as infections by methicillin- and vancomycin-resistant strains of *Staphylococcus aureus* (35, 36). The bactericidal activity of fosfomycin is based on the inhibition of MurA (37) by the irreversible alkylation of an active site cysteine residue, preventing the first step in peptidoglycan synthesis in which phosphoenolpyruvate is linked to the 3′-hydroxyl group of UDP-N-acetyl-glucosamine (38). Bacterial resistance to fosfomycin is achieved by mutations in MurA and by alterations in the glycerophosphate transporter (39, 40). Fosfomycin is inactivated by hydrolysis of its epoxide moiety by the thiol transferases FosA and FosB, and the homologous hydratase enzyme FosX (12–15, 41). Two additional enzymes, FomA and FomB, alter the antibiotic by two consecutive phosphorylation steps resulting in a product unable to alkylate the relevant cysteine residue in MurA. The *fomA* and *fomB* genes are found in the fosfomycin biosynthetic gene clusters of *Streptomyces* and *Pseudomonas* and are thought to confer resistance and facilitate transport in these hosts (42, 43).

The phosphate subdivision of the AAK family of enzymes consists of IPK, FomA, and uridine monophosphate kinase (UMPK) (8, 9, 44). These three enzymes catalyze phosphoryl transfer from ATP by nucleophilic attack of an oxygen atom in a phosphate or phosphonate group in a reaction that proceeds through a pentavalent transition state (8, 31, 44). Within this subdivision, the crystal structures of THA IPK•IP•ATP and the modeled structure of *S. wedmorensis* FomA•fosfomycin•MgATP complexes showed excellent alignment of their catalytic residues and respective substrates (31). These similarities between IPK and FomA suggest that IPK might possess promiscuous activity toward fosfomycin, which could serve as the starting point for evolution of fosfomycin resistance in *Streptomyces* and *Pseudomonas* following horizontal transfer of archaeal DNA.

THA IPK phosphorylates monophosphate esters with small isoprenoid and alkyl moieties (9,11). We found that the enzyme also phosphorylates the phosphonate moiety in fosfomycin. The catalytic constants for the reaction, $k_{cat} = 4 \times 10^{-2}$ s^{-1} and K_m = 15 mM are substantially less favorable ($k_{cat}/K_m = 2.6$ M^{-1}s^{-1}) than for phosphorylation of IP ($k_{cat}/K_m = 1.8 \times 10^6$). Although low, the catalytic efficiency for phosphorylation of fosfomycin by THA IPK could serve as starting point for evolution of an enzyme with more potent fosfomycin kinase activity. There are several examples in the literature of enhancement of extrinsic activities by mutation of one or more residues in the active site. For instance, the *E. coli* RTEM β-lactamase increased its cephalosporinase activity 1.4-fold and decreased its primary penicillase activity 3-fold upon placement of the bacterial strain under the selective pressure of cephalosporin C through two mutations in the active site (45). Subsequently, other mutations were found to result in more dramatic enhancements in cephalosphorinase C activity (46, 47, 48).

The low catalytic efficiency for phosphorylation of fosfomycin by IPK results primarily from the conformation of the molecule in the IP binding site relative to the native substrate. This site contains a pocket lined with hydrophobic residues that cradles the aliphatic tail of IP and controls the size of the isoprene moiety that is bound (8, 9). Fosfomycin, although smaller than IP, contains a polar non-planar epoxide group. In FomA, G53, H58 and S142 create a constellation of hydrogen bond donors to the epoxide group and phosphonate groups of fosfomycin. In THA IPK and MTH IPK a glycine replaces S149 (31, Figure S1). In addition, the side chains of T79 and K83 enhance the hydrophilicity of the fosfomycin binding site in FomA. The two binding poses observed during dynamics simulations with THA IPK showed that fosfomycin was displaced by few Angstroms relative to IP in the binding site, which might reflect unfavorable interactions between the hydrophobic pocket and the polar epoxide group. In the catalytically productive pose obtained from the dynamics calculations, the epoxide moiety is oriented toward solvent. In both poses, fosfomycin blocks the binding of IP, consistent with the competitive inhibition profile we observed.

The low level of fosfomycin activity with IPK is consistent with phosphorylation when the molecule is bound in the first pose. In this conformation, a phosphonate oxygen in the antibiotic can form a hydrogen bond with H50, similar to the interaction responsible for orienting IP for nucleophilic attack on ATP. Although the nucleophilic phosphonate group is more distant from the γ phosphate group of ATP than the phosphate moiety in IP in the native reaction (Figure 1b), K5, K14, H50, and K205, which stabilize the transition state for phosphorylation of IP, are engaged in a similar manner in the first pose for fosfomycin. Thus, this pose can be reasonably assigned as the productive ternary complex (Figure 4d). K14 and H50, which are invariant among all IPKs and FomAs, appear to be particularly important. K14 binds the phosphate group of ATP in the IPK•IP•ATP complex and is positioned to stabilize the highly negatively charged transition state (8). The K14A mutation results in doubling of K_m^{ATP} and a 460-fold decrease in k_{cat}^{IP}(Figure S8 and Table S1). A

K18A mutation of the corresponding residue in FomA inactivates the enzyme (31). Both productive and dead end complexes of fosfomycin in IPK show K14 in almost identical conformations suitable for transition state stabilization (Figure 4d and 4e). H50 in THA IPK hydrogen bonds with the terminal phosphate groups of IP and the product IPP (8), and mutagenesis studies of the corresponding residues in *M. jannaschii* IPK (H60) and *S. wedmorensis* FomA (H58) showed that this interaction is important for transition state stabilization accompanying the nucleophilic displacement of ADP (9, 31). These structural and kinetic data strongly indicate that the first binding pose that contains the H50-phosphonate hydrogen bond is a productive complex.

Our results are consistent with the proposal that FomA might be descended from an archaeal IPK following horizontal transfer of an archaeal *ipk* gene to *Streptomyces* and subsequent adaptive mutations that confer antibiotic resistance. Evolution of FomA from IPK by enhancement of the promiscuous fosfomycin kinase activity seen for IPK would provide a selective advantage for the fosfomycin synthesizing bacterium (4). Low levels of activity similar to that we found for fosfomycin kinase activity in IPK ($k_{cat}/K_m = 2.8 \times 10^6\ M^{-1}s^{-1}$) have been shown to confer an immediate selective advantage. For example, phosphonate monoester hydrolase in *Burkholderia caryophili* ($k_{cat}/K_m = 9.5\ M^{-1}s^{-1}$) allowed this organism to thrive on glyceryl glyphosate, a previously unencountered phosphorous source (50–52). A catalytic efficiency of only $0.3\ M^{-1}s^{-1}$ (*E. coli* glutamine phosphoribosylpyrophosphate amidotransferase) provided a similar advantage, although it was necessary to overexpress the gene from a multicopy plasmid under control of a strong promoter (53). Likely instances of horizontal transfer of metabolic genes between *Archaea* and *Bacteria* (and other inter-domain HGTs) have been proposed for acquisition of mevalonate pathway genes from *Archaea* (or Eukarya) by *Borrelia* and *Cocci* and for acquisition of the bacterial glycerol dehydrogenase gene by Archaea (54).

Supplementary Material

Refer to Web version on PubMed Central for supplementary material.

Acknowledgments

Funding

This research was supported by NIH Grant GM 25521 (C. D. P.)

We thank Dr. Kate Slessor for the purified S. *wedmorensis* FomA used in the product turnover assay. We also thank Dr. James Muller and Dr. Jian-Jung Pan for assistance in the MS/MS fragmentation experiment.

ABBREVIATIONS

AAK	amino acid kinase
THA	Thermoplasma acidophilum
IPK	isopentenyl phosphate kinase
FomA	fosfomycin kinase
NAGK	N-acetyl-L-glutamate kinase
UMPK	uridine monophosphate kinase
IP	isopentenyl monophosphate
IPP	isopentenyl diphosphate

ATP adenosine triphosphate

References

1. Blume-Jensen P, Hunter T. Oncogenic kinase signaling. Nature. 2001; 411:355–365. [PubMed: 11357143]
2. Jensen RA. Enzyme recruitment in evolution of new function. Annu Rev Microbiol. 1976; 30:409–425. [PubMed: 791073]
3. Ohno, S. Evolution by gene duplication. George Allen and Unwin; London: 1970.
4. O'Brien PJ, Herschlag D. Catalytic promiscuity and the evolution of new enzyme activities. Chem Biol. 1999; 6:R91–R105. [PubMed: 10099128]
5. Copley S. Enzymes with extra talents: moonlighting functions and catalytic promiscuity. Curr Opin Chem Biol. 2003; 7:265–272. [PubMed: 12714060]
6. Yang K, Metcalf WW. A new activity for an old enzyme: Escherichia coli bacterial alkaline phosphatase is a phosphite-dependent hydrogenase. Proc Natl Acad Sci. 2004; 101(21):7919–7924. [PubMed: 15148399]
7. Miller BG, Raines RT. Reconstitution of a defunct glycolytic pathway via recruitment of ambiguous sugar kinases. Biochemistry. 2005; 44:10776–10783. [PubMed: 16086580]
8. Mabanglo MF, Schubert HL, Chen M, Hill CP, Poulter CD. X-ray structures of isopentenyl phosphate kinase. ACS Chemical Biology. 2010; 5(5):517–527. [PubMed: 20402538]
9. Dellas NP, Noel JP. Mutation of archaeal isopentenyl phosphate kinase highlights mechanism and guides phosphorylation of additional isoprenoid monophosphates. ACS Chemical Biology. 2010; 5(6):589–601. [PubMed: 20392112]
10. Pakhomova S, Bartlett S, Augustus A, Kuzuyama T, Newcomer M. Crystal structure of fosfomycin resistance kinase FomA from *Streptomyces wedmorensis*. J Biol Chem. 2008; 283:28518–28526. [PubMed: 18701452]
11. Chen M, Poulter CD. Characterization of thermophilic archaeal isopentenyl phosphate kinases. Biochemistry. 2010; 49:207–217. [PubMed: 19928876]
12. Dela Cruz, F.; Garcia-Lobo, JM.; Davies, J. Bacterial resistance to antimicrobials. Lewis, K.; Salyers, AA.; Taber, HW.; Wax, RG., editors. Marcel Dekker, Inc; New York, NY: 2002. p. 19-36.
13. Suarez JE, Mendoza MC. Plasmid-encoded fosfomycin resistance. Antimicrob Agents Chemother. 1991; 35:791–795. [PubMed: 1854159]
14. Bernat BA, Laughlin LT, Armstrong RN. Fosfomycin resistance protein (FosA) is a manganese metalloglutathione transferase related to glyoxalase I and the extradiol dioxygenases. Biochemistry. 1997; 36:3050–3055. [PubMed: 9115979]
15. Cao M, Bernat BA, Wang Z, Armstrong RN, Helmann JD. FosB, a cysteine-dependent fosfomycin resistance protein under the control of sigma (W), an extracytoplasmic-function sigma factor in *Bacillus subtilis*. J Bacteriol. 2001; 183:2380–2383. [PubMed: 11244082]
15. Etienne J, Gerbaud G, Courvalin P, Fleurette J. Plasmid-mediated reistance to fosfomycin in *Staphylococcus epidermidis*. FEMS Microbiol Lett. 1989; 52:133–137. [PubMed: 2599353]
16. Etienne J, Gerbaud G, Courvalin P, Fleurette J. Plasmid-mediated resistance to fosfomycin in Staphylococcus epidermids. FEMS Microbiol Lett. 1989; 52:133–137. [PubMed: 2599353]
17. Pilloff D, Dabovic K, Romanovski MJ, Nonanno JB, Doherty M, Burley SK, Leyh TS. The kinetic mechanism of phosphomevalonate kinase. J Biol Chem. 2003; 278:4510–4515. [PubMed: 12424232]
18. Leatherbarrow, RJ. GraFit Version 5. Erithacus Software Ltd; Horley, U.K: 2001.
19. Zewe V, Fromm HJ. Kinetic studies of rabbit muscle lactate dehydrogenase. Biochemistry. 1965; 4(4):782–792. [PubMed: 14323584]
20. Lindahl, E.; Hess, B.; van der Spoel, D. GROMACS 3.0: a package for molecular simulation and trajectory analysis. Springer; Berlin/Heidelberg: 2001. p. 306-317.

21. MacKerell AD Jr, Bashford D, Bellott M, Dunbrack RL Jr, Evanseck J, Field MJ, Fischer S, Gao J, Guo H, Ha S, Joseph D, Kuchnir L, Kuczera K, Lau FTK, Mattos C, Michnick S, Ngo T, Nguyen DT, Prodhom B, Reiher WE III, Roux B, Schlenkrich M, Smith J, Stote R, Straub J, Watanabe M, Wiorkiewicz-Kuczera J, Yin D, Karplus M. All-atom empirical potential for molecular modeling and dynamics studies of proteins. J Phys Chem B. 1998; 102:3586–3616.
22. Zoete, V.; Cuendet, MA.; Grosdidier, A.; Michielin, O. SwissParam, a Fast Force Field Generation Tool For Small Organic Molecules. to be submitted
23. Jorgensen WL, Chandrasekhar J, Madura JD, Impey RW, Klein ML. Comparison of simple potential functions for simulating liquid water. J Chem Phys. 1983; 79:926–935.
24. Ramon-Maiques S, Marina A, Gil-Ortiz F, Fita I, Rubio V. Structure of acetylglutamate kinase, a key enzyme for arginine biosynthesis and a prototype for the amino acid kinase family, during catalysis. Structure. 2002; 10:329–342. [PubMed: 12005432]
25. Davis IW, Leaver-Fay A, Chen VB, Block J, Kapral GJ, Wang X, Murray L, Arendall B III, Snoeyink J, Richardson JS, Richardson DC. Molprobity: all-atom contacts and structure validation for proteins and nucleic acids. Nucleic Acids Res. 2007; 35:W375–W383. Web Server Issue. [PubMed: 17452350]
26. Essman U, Perera L, Berkowitz ML, Darden T, Lee H, Pedersen LG. A smooth particle mesh Ewald potential. J Chem Phys. 1995; 103:8577–8592.
27. Bussi G, Donadio D, Parrinello M. Canonical sampling through velocity rescaling. J Chem Phys. 2007; 126:012101.
28. Parrinello M, Rahman A. Polymorphic transitions in single crystals: A new molecular dynamics method. J Appl Phys. 1981; 52:7182–7190.
29. Knowles JR. Enzyme-catalyzed phosphoryl transfer reactions. Annu Rev Biochem. 1980; 49:877–819. [PubMed: 6250450]
30. O'Brian CA, Ward NE. Characterization of calcium- and phospholipid-dependent ATPase reaction catalyzed by rat brain protein kinase C. Biochemistry. 1990; 29:4278–4282. [PubMed: 2161679]
31. Pakhomova S, Bartlett S, Doerner PA, Newcomer M. Structural and biochemical insights into the mechanism of fosfomycin phosphorylation by fosfomycin resistance kinase FomA. Biochemistry. 2011; 50(32):6909–6919. [PubMed: 21728358]
33. Shoji J, Kato T, Hinoo H, Hattori T, Hirooka K, Matsumoto K, Tanimoto T, Kondo E. Production of fosfomycin (phosphonomycin) by *Pseudomonas syringae*. J Antibiot (Tokyo). 1986; 39:1011–1012. [PubMed: 3759643]
34. Lobel B. Short-term therapy for uncomplicated urinary tract infection today. Clinical outcome upholds the theories. Int J Antimicrob Agents. 2003; 22(Suppl 2):85–87. [PubMed: 14527777]
35. Cassone M, Campanile F, Pantosti A, Venditti M, Stefani S. Identification of a variant "Rome clone" of methicillin-resistant *Staphylococcus aureus* in France: a phylogenetic approach. Microb Drug Resist. 2004; 10:43–49. [PubMed: 15140393]
36. Nakazawa H, Kikuchi Y, Honda T, Isago T, Nozaki M. Enhancement of antimicrobial effects of various antibiotics against methicillin-resistant Staphylococcus aureus (MRSA) by combination with fosfomycin. J Infect Chemother. 2003; 9:304–309. [PubMed: 14691650]
37. Kahan FM, Kahan JS, Cassidy PJ, Kropp H. The mechanism of action of fosfomycin (phosphonomycin). Ann NY Acad Sci. 1974; 235:364–386. [PubMed: 4605290]
38. Marquardt JL, Brown ED, Lane WS, Haley TM, Ichikawa Y, Wong CH, Walsh CT. Evidence that the fosfomycin target Cys115 in UDP-N-acetylglucosamine enolpyruvyl transferase (MurA) is essential for product release. Biochemistry. 1994; 33:10646–10651. [PubMed: 8075065]
39. Kadner RJ, Winkler HH. Isolation and characterization of mutations affecting the transport of hexose phosphates in Escherichia coli. J Bacteriol. 1973; 113:895–900. [PubMed: 4347928]
40. Tsuruoka T, Yamada Y. Characterisation of spontaneous fosfomycin (phosphonomycin)-resistant cells of *Escherichia coli* B "in vitro". J Antibiot (Tokyo). 1975; 28:906–911. [PubMed: 1104551]
41. Nair SK, van der Donk WA. Structure and mechanism of enzymes involved in biosynthesis and breakdown of the phosphonates fosfomycin, dehydrophos, and phosphinothricin. Arch Biochem Biophys. 2010; 505(1):13–21. [PubMed: 20854789]

42. Kobayashi S, Kuzuyama T, Seto H. Characterization of the *fomA* and *fomB* gene products from *Streptomyces wedmorensis*, which confer fosfomycin resistance on *Escherichia coli*. Antimicrob Agents Chemother. 2000; 44:647–650. [PubMed: 10681332]
43. Woodyer RD, Shao Z, Thomas PM, Kelleher NL, Blodgett JA, Metcalf WW, van der Donk WA, Zhao H. Heterologous production of fosfomycin and identification of the minimal biosynthetic gene cluster. Chem Biol. 2006; 13:1171–1182. [PubMed: 17113999]
44. Marco-Marin C, Gil-Ortiz F, Rubio V. The crystal structure of *Pyrococcus furiosis* UMP kinase provides insight into catalysis and regulation in microbial pyrimidine nucleotide biosynthesis. J Mol Biol. 2005; 352:438–454. [PubMed: 16095620]
45. Hall A, Knowles JR. Directed selective pressure on a beta-lactamase to analyse molecular changes involved in development of enzyme function. Nature. 1976; 264:803–804. [PubMed: 796732]
46. Healey WJ, Labgold MR, Richards JH. Substrate specificities in class A beta-lactamases: preference for penams vs. cephems The role of residue 237. Proteins. 1989; 6:275–283. [PubMed: 2622907]
47. Gibson RM, Christensen H, Waley SG. Site-directed mutagenesis of beta-lactamase I. Single and double mutants of Glu-166 and Lys-73. Biochem J. 1990; 272:613–619. [PubMed: 1980064]
48. Imtiaz U, Manavathu EK, Lerner SA, Mobashery S. Critical hydrogen bonding by Serine 235 for cephalosporinase activity by TEM1 beta-lactamase. Antimicrob Agents Chemother. 1993; 37:2438–2442. [PubMed: 8285630]
49. Boucher, Y. Lipids: biosynthesis, function, and evolution in Archaea. In: Cavicchioli, R., editor. Molecular and Cellular Biology. ASM Press; Washington, DC: 2007. p. 341-353.
50. Van Loo B, Jonas S, Babtie AC, Benjdia A, Berteau O, Hyvönen M, Hollfelder F. An efficient, multiply promiscuous hydrolase in the alkaline phosphatase family. Proc Natl Acad Sci USA. 2010; 107(7):2740–2745. [PubMed: 20133613]
51. Ghanem E, Li Y, Xu C, Raushel FM. Characterization of a phosphodiesterase capable of hydrolyzing EA 2192, the most toxic degradation product of the nerve agent VX. Biochemistry. 2007; 46:9032–9040. [PubMed: 17630782]
52. McLoughlin SY, Jackson C, Liu JW, Ollis DL. Growth of *Escherichia coli* co-expressing phosphotriesterase and glycerophosphodiester phosphodiesterase, using paraoxon as the sole phosphorous source. Appl Environ Microbiol. 2004; 70:404–412. [PubMed: 14711669]
53. Patrick WM, Matsumura I. A study in molecular contingency: glutamine phosphoribosylphosphate amidotransferase is a promiscuous and evolvable phosphoribosylanthranilate isomerase. J Mol Biol. 2008; 377:323–336. [PubMed: 18272177]
54. Boucher Y, Kamekura M, Doolittle WF. Origins and evolution of isoprenoid lipid biosynthesis in Archaea. Mol Microbiol. 2004; 52(2):515–527. [PubMed: 15066037]

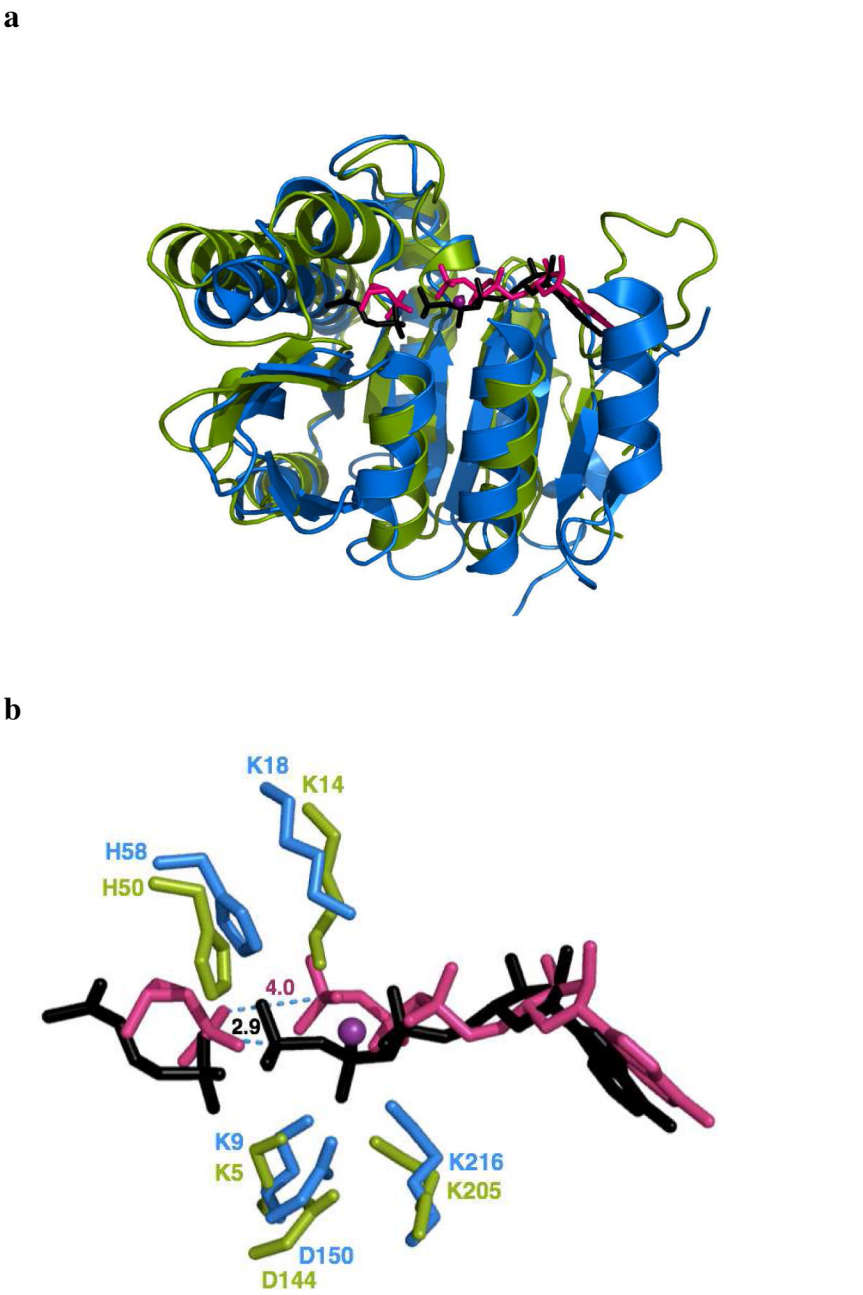

Figure 1.

T. acidophilum IPK and *S. wedmorensis* FomA have high structural homology. (a) Superimposed crystal structures of IPK (3LKK, green) and FomA (3QUO, blue) have RMSD of 2.6 Å over 224 amino acid residues. The substrates of IPK (IP and ATP, black) and FomA (fosfomycin and ATP, pink) also align well in their respective active sites. The divalent metal Mg^{2+} is shown as a purple sphere. (b) Alignment of catalytic residues invariant in IPK and FomA, suggesting similar mechanisms of phosphoryl transfer. The FomA•fosfomycin•MgATP complex was modeled using the structures of the FomA•MgATP (3QUN) and FomA•fosfomycin•ATP (3QUO) complexes. Hydrogen bond lengths are indicated.

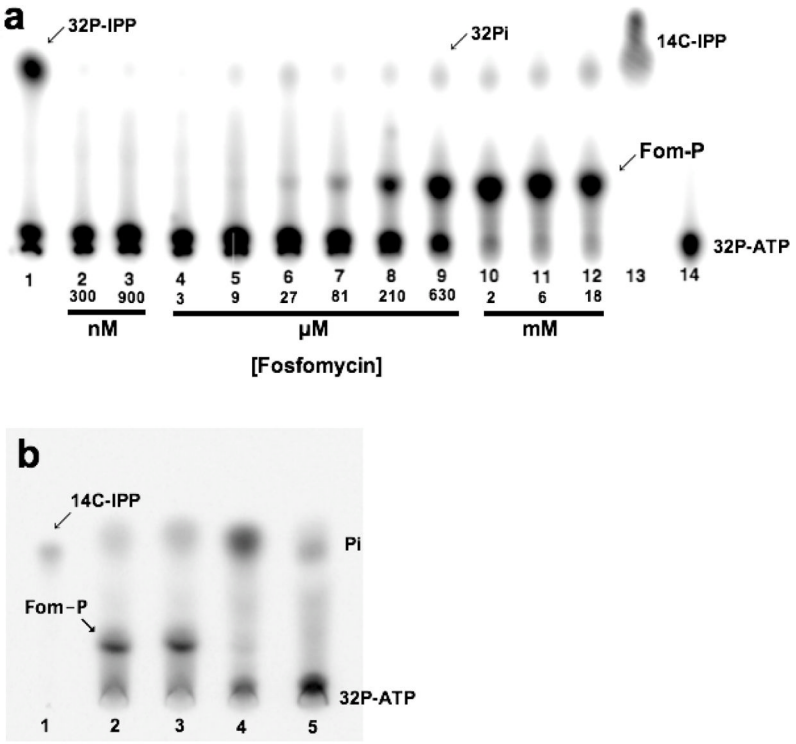

Figure 2.

Autoradiograms showing that IPK can phosphorylate fosfomycin in the presence of ATP. (a) Product turnover assay of THA IPK using IP or fosfomycin as substrates. The product of the native reaction, [^{32}P] IPP, and the by-product of the intrinsic ATPase activity, ^{32}Pi, migrate with almost similar R_fs. This ATPase activity is independent of fosfomycin concentration. Increasing phosphorylation of fosfomycin is observed in the μM to mM range. All lanes except lane 13 contained γ-[^{32}P] ATP and 200 nM IPK. (1) 3.5 μM IP and IPK, (2) 300 nM fosfomycin, (3) 900 nM, (4) 3 μM, (5) 9 μM, (6) 27 μM, (7) 81 μM, (8) 210 μM, (9) 630 μM, (10) 2 mM, (11) 6 mM, (12) 18 mM, (13) [^{14}C-IPP] (14) γ-[^{32}P] ATP and IPK. (b) Comparison of the products of *S. wedmorensis* FomA and THA IPK (20 μM each) upon incubation with fosfomycin. All lanes except lane 1 contained γ-[^{32}P] ATP. (1) [^{14}C] IPP standard. (2) *S. wedmorensis* FomA and 10 mM fosfomycin, (2) THA IPK and 10 mM fosfomycin, (3) *S. wedmorensis* FomA incubated without fosfomycin, and (4) incubation including 10 mM fosfomycin but with neither *S. wedmorensis* FomA or THA IPK.

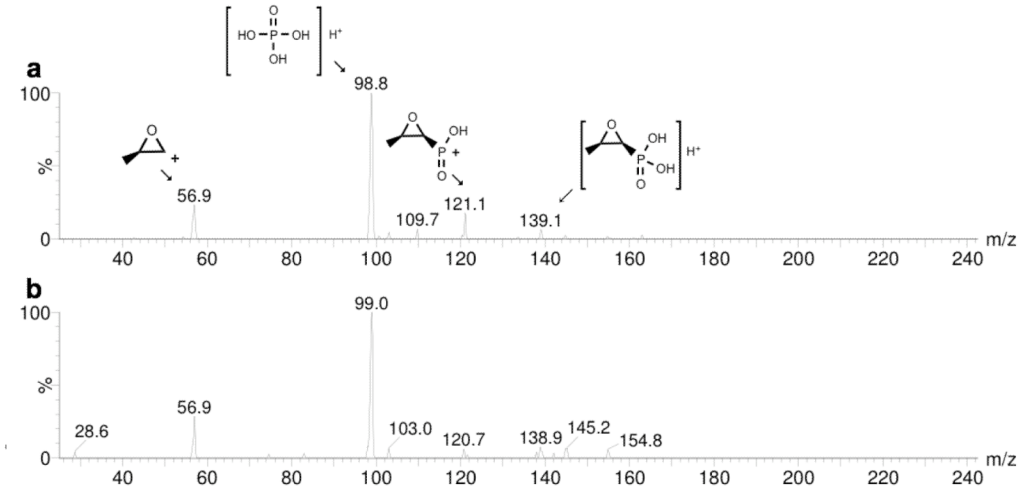

Figure 3.

MS/MS fragmentation of the ammonium form of fosfomycin phosphate (mass 236) produced by THA IPK and *S. wedmorensis* FomA. (a) Fragmentation of the product formed by THA IPK showed peaks corresponding to $[C_3H_5O]^+$ (56.9), $[H_4O_4P]^+$ (98.8), $[C_3H_6O_3P]^+$ (121.1) and $[C_3H_8O_4P]^+$ (139.1). The same peaks were found in the fragmentation of product formed by *S. wedmorensis* FomA (b).

a

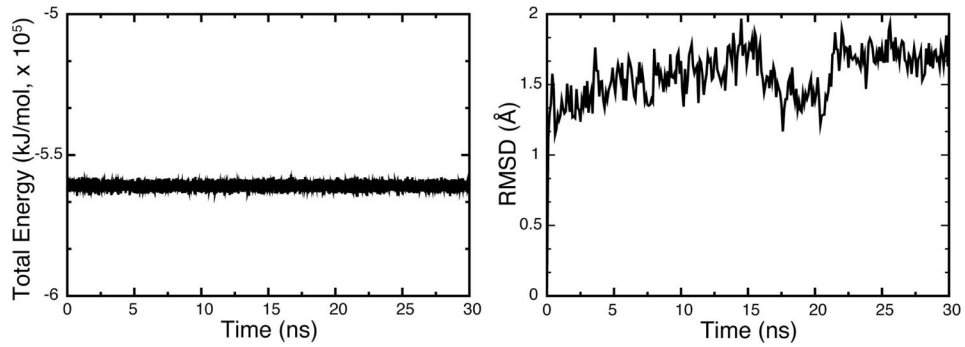

b

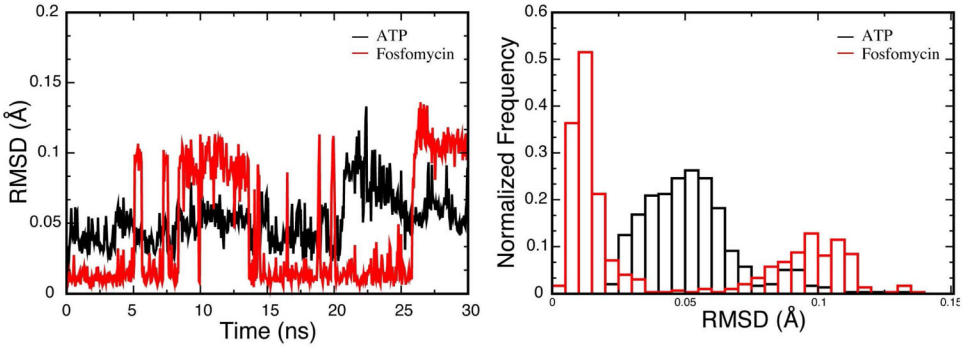

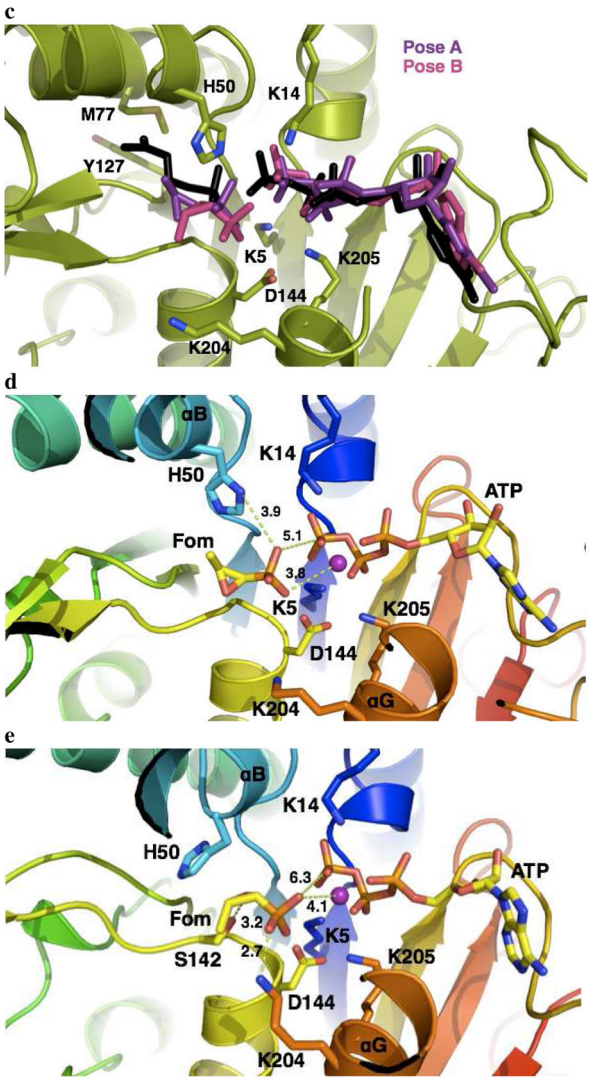

Figure 4.

The IPK•fosfomycin•MgATP complex is stable with two binding poses for fosfomycin in the IP binding site. (a) Energy (left) and RMSD time-series (right) showing that the modeled IPK•fosfomycin•MgATP complex is stable. (b) Ligand (fosfomycin and ATP, left) RMSD and histogram (right) showing a two-state binding conformation for fosfomycin, while ATP is essentially fixed. (c) Superposition of the native IPK•IP•ATP complex (substrates IP and ATP in black) with the two binding poses of fosfomycin near the IP binding site. In both binding poses, fosfomycin is translated by an average of 4 Å to relieve unfavorable interactions with the hydrophobic IP binding site. M77 and Y127 immediately below the aliphatic tail of IP are shown. (d) The productive complex, IPK•fosfomycin•MgATP, similar to the native IPK•IP•ATP complex, with Mg^{2+} and the phosphonate group engaging in electrostatic interactions. (e) The dead-end complex where S142 and K204 donate hydrogen bonds to fosfomycin, forming a stable complex.

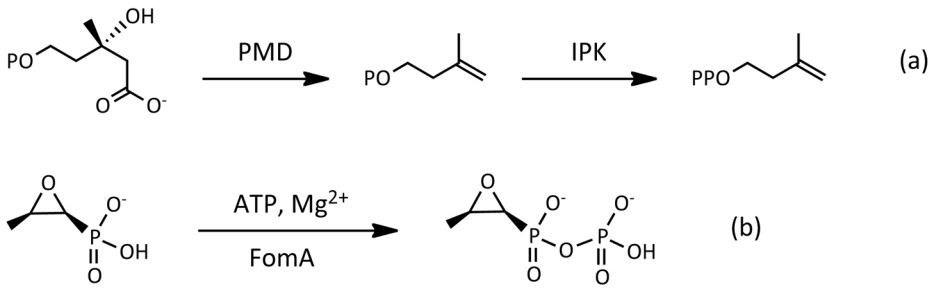

Scheme 1.

Phosphoryl transfer reactions catalyzed by IPK and FomA. (a) The alternate route in the archaeal mevalonate pathway proceeds with the decarboxylation of mevalonate phosphate by phosphomevalonate decarboxylase (PMD) to form isopentenyl phosphate IP, followed by phosphorylation by IPK to form the isoprene unit IPP. (b) FomA inactivates fosfomycin by phosphorylation using ATP as donor. A second phosphorylation step by the enzyme FomB (not shown) completes the inactivating covalent modifications of the antibiotic.

Table 1

Steady state kinetic constants for phosphorylation of IP and fosfomycin.

	IP Wild type IPK	Fosfomycin Wild type IPK	IP K204A	Fosfomycin K204A
k_{cat} (s^{-1})	8.0 ± 0.2	(4 ± 0.1) × 10^{-2}	7.7 ± 0.2	(3 ± 0.1) × 10^{-2}
K_m (μM)	4.4 ± 0.5	(1.5 ± 0.1) × 10^4	2.8 ± 0.3	(1.1 ± 0.1) × 10^4
k_{cat}/K_m ($M^{-1}s^{-1}$)	1.8 × 10^6	2.6	2.8 × 10^6	2.5
K_m^{ATP} (μM)	6.0 ± 0.5	1.4 ± 0.1	6.9 ± 0.6	1.2 ± 0.2
K_d (μM)	4.6 ± 1.5	(1.8 ± 0.3) × 10^4	4.6 ± 1.3	(1.5 ± 0.5) × 10^4